Scripta Materialia 203 (2021) 114065

Contents lists available at ScienceDirect

Scripta Materialia

journal homepage: www.elsevier.com/locate/scriptamat

Substantial role of charge transfer on the diffusion mechanism of interstitial elements in α-titanium: A First-principles study

Kazuki Shitara[a,*], Masato Yoshiya[b], Junko Umeda[a], Katsuyoshi Kondoh[a]

[a] Joint and Welding Research Institute, Osaka University, Ibaraki, 567-0047, Japan
[b] Division of Materials and Manufacturing Science, Graduate School of Engineering, Osaka University, Suita, 565-0871, Japan

ARTICLE INFO

Article history:
Received 5 February 2021
Revised 1 June 2021
Accepted 3 June 2021
Available online 19 June 2021

Keywords:
Titanium
Diffusion mechanism
First-principles calculations

ABSTRACT

The diffusion mechanism of interstitial solute elements in α-Ti was investigated using first-principles calculations. Solute elements, B, C, N, O and F, were confirmed to be ~~the~~ most stable at octahedral sites with their calculated formation energies. The migration energies of C, N and O are high, approximately 2 eV, while those of B and F were approximately 1 eV. A high correlation was observed between the migration energies and difference in the charge densities of the solute atoms between stable and transition states. These results indicate that migration energies and resultant diffusion could not be determined only by the atomic radii of solute atoms, and charge transfer must also be taken into consideration. The charge transfer between matrix and solute atoms affects diffusion mechanism of solute atoms in Ti.

© 2021 Acta Materialia Inc. Published by Elsevier Ltd. All rights reserved.

Main text

Recently, there have been efforts to simultaneously achieve high strength and ductility of Ti-based alloys by controlling their microstructures [1–3], including the exploitation of bimodal phase distributions in which each phase plays a selective role, such as the α- and β-phases in Ti–6Al–4V [4–8]. The use of solute elements could also be optimized to promote a more desired balance of mechanical properties. For decades, there have been extensive research on the impact of solute elements, such as O and N, on the microstructure and resultant mechanical properties of pure Ti [9–18]. The diffusion of interstitial elements is also related to the partitioning and microstructures evolution in Ti alloys, whose changes involve thermodynamically modification and thus have great influence on the mechanical properties of the alloys. In the Ti-6Al-4V based alloy, for example, fast diffusion rate of O causes O-rich region at the interfaces between ω- and β-phases, which become preferential nucleation sites of α-phase [19]. Some recent studies about the additive manufacturing can achieve the three-dimensionally controlled non-equilibrium microstructure due to fast-quenching solidification [20–23], implying the importance of diffusion of O and N which are easily absorbed in the alloys even from the controlled atmosphere during materials processing and adsorbed on surfaces of starting powders. However, it remains challenging to precisely understand the kinetics, especially in the case of interstitial elements, due to rapid diffusions of these species.

Typical solute elements, such as O and N, either remain or are often entrapped in Ti during materials processing, like C in steel. Thus, there have been several extensive experimental and computational studies on the diffusion of the typical elements in Ti [24–37]. The activation energies of diffusion reported ranges between 1.17, 1.35 ~ 1.89, 1.45 ~ 2.13 or 1.96 ~ 2.32 eV for B, C, O or N [25,26,30–36,38], respectively. To theoretically clarify the diffusion mechanism, Wu and Trinkle calculated the diffusivity and examined diffusion mechanism of O in α-Ti using first-principles calculations [27], revealing that O diffuses from octahedral site to octahedral sites via hexahedral or crowdion sites. Scotti and Mottura have reported the migration mechanism of C, N and O by the combination of first-principles calculation and kinetic Monte Carlo method [29]. Moreover, the fast diffusion of some of substitutional elements such as Fe, Co and Ni is also related with the interstitial diffusion mechanism [24,25,39].

It is widely accepted that an atom at an interstitial site can diffuse throughout lattice significantly faster than that at a substitutional site [24,25] as there is no need for a vacancy at the next site. One may think that atomic size determines the energy barrier for diffusion; its small size allows the atom to reside at an interstitial site even for metallic materials with free-like electrons. However, it is often overlooked that the difference in the electronegativity between the host Ti and interstitial solute elements is greater than that between Ti and substitutional elements, resulting in the partial ionization of atoms. In fact, N has a smaller atomic radius

* Corresponding author.

https://doi.org/10.1016/j.scriptamat.2021.114065
1359-6462/© 2021 Acta Materialia Inc. Published by Elsevier Ltd. All rights reserved.

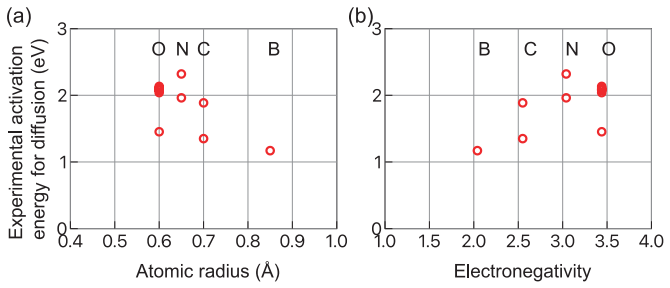

Fig. 1. Experimentally-reported activation energies for diffusion of interstitial solute elements in α-Ti [25,26,30–36,38,41] as functions of (a) atomic radius [40] and (b) Pauling's electronegativity [42].

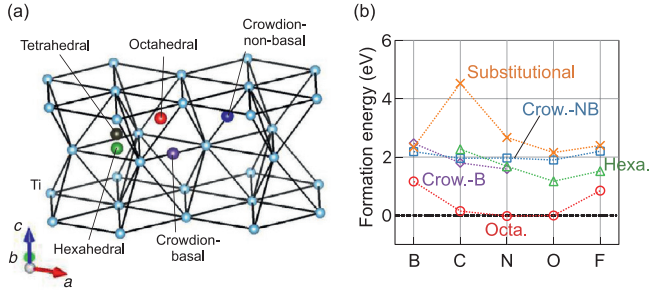

Fig. 2. (a) Schematic crystal structures showing the interstitial sites for solutes in α-Ti. (b) Formation energies of the point defects for each solute element obtained by the first-principles calculations. Circle, triangle, diamond, square and cross symbols denote octahedral, hexahedral, basal crowdion, non-basal crowdion and substitutional sites, respectively. Crow.-B and Crow.-NB denote the basal crowdion and non-basal crowdion sites, respectively. The dotted lines are drawn for the stable interstitial sites obtained in this study only to serve as a guide. The solute elements were found to be most stable at the octahedral site.

but a lower diffusion coefficient than C [25,40]. Fig. 1 shows the experimentally-reported activation energies of diffusion [25,26,30–36,38,41] as functions of the atomic radius[40] and Pauling's electronegativity [42]. The non-monotonic dependence can be seen for each elemental parameter, suggesting the energy barrier for diffusion cannot be simply interpreted by these elemental parameters alone. Though the diffusion mechanism was investigated as mentioned above, the origin of the difference in the activation energies between these interstitial solutes has not been understood yet. In these regards, transition of electronic states in the course of diffusion, especially transition of interatomic bonds between hopping interstitial atoms and host atoms with their distance being changed upon diffusion, needs to be more carefully examined to identify the extra factor that dictates the diffusion.

In this study, we fully investigated the solid solution state of interstitial solute elements and their diffusion mechanism in α-Ti by first-principles calculations. Particularly, we focused on the role on diffusion not only of the elemental features, such as atomic radius and electronegativity, but also of the charge transfer with the host Ti atoms.

The formation energies of the point defects were evaluated using the first-principles calculations. A supercell model with $4 \times 4 \times 3$ optimized unit cells, which was determined from the convergence of defect formation energy for the O atom at the octahedral site, was constructed with fully relaxed atomic positions. In this study, not only octahedral and tetrahedral but also hexahedral, basal crowdion and non-basal crowdion sites were investigated as interstitial sites, in addition to substitutional site. The interstitial siters are shown in Fig. 2(a). To remove the symmetry constraints, the solute atoms in the supercells were intentionally randomly displaced within 0.05 Å from its equilibrium position. Formation energies were calculated using pure-Ti and stable compounds of solutes on the convex hull in free energy plots as a function of composition for each binary system. Details are described in the Supplementary Materials (S2). The first-principles calculations were performed using the projected augmented wave (PAW) method as implemented in the VASP code [43–46]. The exchange-correlation term was treated with the Perdew–Burke–Ernzerhof functional [47]. The 3*s*, 3*p*, 4*s* and 3*d* electrons of the Ti atoms, and 2*s* and 2*p* electrons of solute atoms were treated as valence electrons for all calculations. The plane wave cutoff energies were set to 520 eV. The integration in the reciprocal space was performed with $3 \times 3 \times 3$ Γ-point-centered Monkhorst-Pack grids [48]. Structure optimization was carried out until all residual forces acting on each atom were less than 1 meV/Å. Only internal atomic positions are relaxed assuming infinitely dilute states, where the effect of cell volume and shape changes were negligible.

Fig. 2(b) shows the formation energies of the point defects calculated by the first-principles calculations. Even in static calculations, the solute atom at some interstitial sites in the initial structure moved to other interstitial sites in the optimized structure. For example, B at the tetrahedral site in the initial structure moved to the octahedral site after structure optimization, i.e. B at the tetrahedral site is unstable. These moved atoms from the initial sites were not plotted in Fig. 2(b). The obtained stable sites for interstitials are summarized in Table S1. All solute elements were found to be most stable at the octahedral site. The formation energies of B and F at the octahedral sites calculated as largely positive (1 eV). The former corresponds to the inability of B to dissolve in Ti, as reported in the phase diagram [49].

Based on the stable sites for each solute atom, the candidates for the diffusion paths were constructed (Table S2). Since the octahedral sites were the most stable for all solute elements, they were included in all diffusion paths. The migration energies were calculated using the climbing image nudged elastic band (CI-NEB) method with an intermediate image [50–58]. Only the atomic positions were relaxed in the CI-NEB calculations. As the simple transition between stable sites at close distances involving one interstitial solute atom was considered in this study, one intermediate image could sufficiently estimate the migration energies according to preceding studies [27,28]. Fig. 3(a) shows the migration energies for the diffusion paths. The lowest migration energies were calculated to be 1.09, 1.84, 2.18, 1.99 and 1.14 eV for B, C, N, O and F, respectively. For solutes B, C and O, the diffusion path with the lowest migration energy was from the octahedral to non-basal crowdion sites, though the diffusion path for C and O had a nearly equal migration energy from the octahedral to basal crowdion sites and from the octahedral to hexahedral sites, respectively. The solutes N and F diffused with the lowest migration energy from the octahedral to hexahedral sites with N having almost the same energy for the diffusion path from the octahedral to basal crowdion sites. As mentioned earlier, the activation energies of diffusion coefficients were experimentally reported as 1.17, 1.35 ~ 1.89, 1.96 ~ 2.32 and 1.45 ~ 2.13 eV for B, C, N and O, respectively [25,26,30–36,38,41]. The order of activation energies; N, O, C and B, is now in accordance with the calculated migration energies.

Fig. 3(b-d) shows the schematic illustrations of the diffusion paths obtained throughout the crystal. For long-range diffusion, the solute atoms migrated along (i) a one-dimensional path along the *c*-axis via the octahedral and basal crowdion sites, (ii) a two-dimensional path on the *ab*-plane via the octahedral and non-basal crowdion sites and (iii) a three-dimensional path via the octahedral and hexahedral sites. Experimental data on anisotropy of the O diffusion reveals that it is slightly easier for O to diffuse along *c*-axis than on *ab*-plane [37]. The experimentally observed anisotropy is consistent with our result; (ii) the two-dimensional path on *ab*-plane from octahedral to non-basal crowdion sites with the lowest

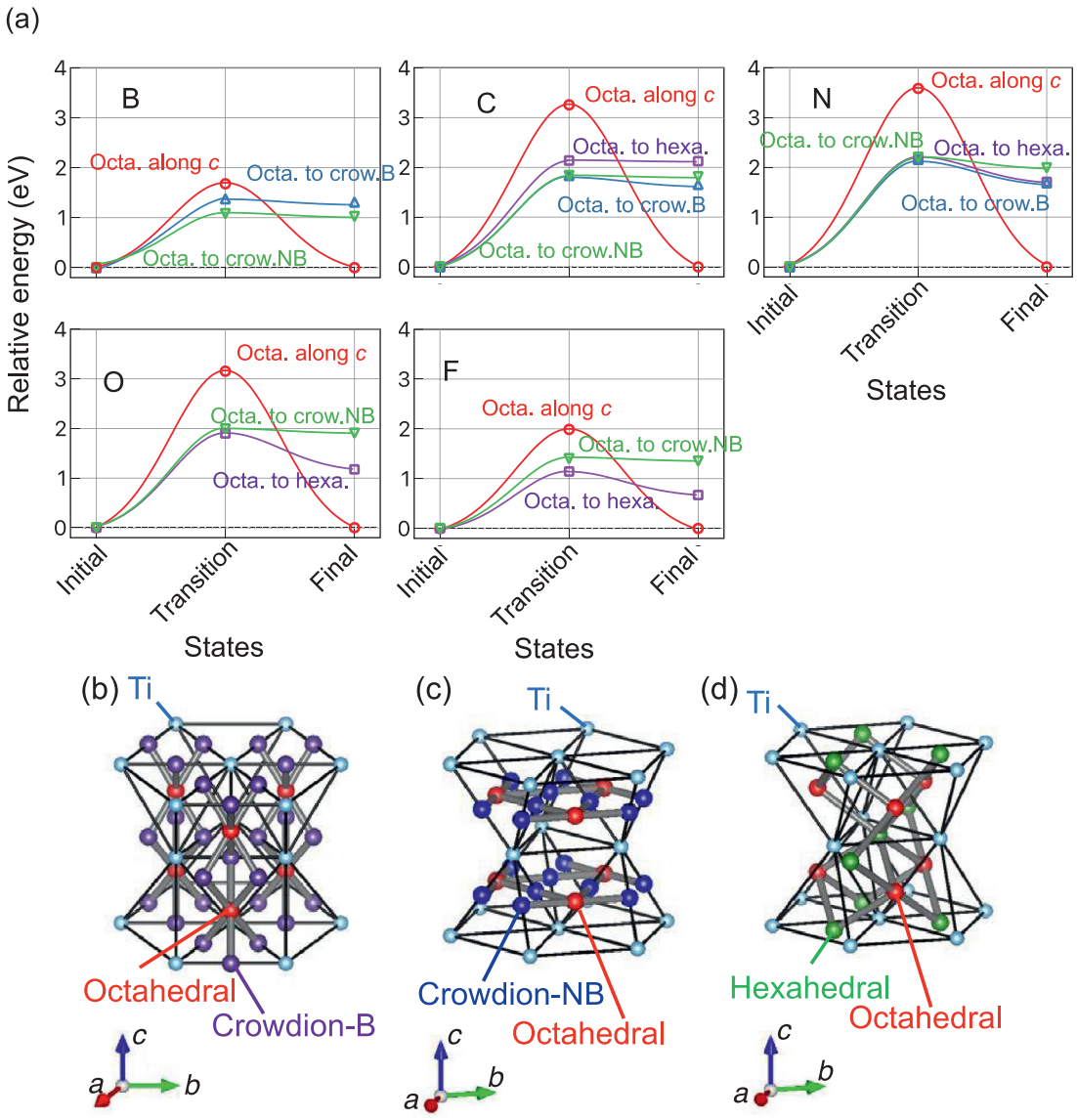

Fig. 3. (a) Calculated migration energies for the interstitial solute atoms by the climbing nudged elastic band method. Circle, square, upward triangle and downward triangle symbols denote the path from octahedral to octahedral sites along *c*-axis, to hexahedral sites, to basal crowdion sites and to non-basal crowdion sites, respectively. The curve lines connecting the stable and transition points are provided only to serve as a guide. (b-d) Identified long-range diffusion paths (b) from the octahedral to basal-crowdion, (c) from the octahedral to non-basal-crowdion and (d) from the octahedral to hexahedral sites. For the long-range diffusion, solute atoms migrate on a one-dimensional path along the *c*-axis via the octahedral and basal crowdion sites, two-dimensional path on the *ab*-plane via the octahedral and non-basal crowdion sites, and three-dimensional path via the octahedral and hexahedral sites.

migration energy, (iii) the three-dimensional path from the octahedral to hexahedral sites with almost the same energy as the lowest one and (i) one-dimensional path along *c*-axis with much higher migration energy among the assumed paths. The O diffusion in the two-dimensional path on *ab*-plane will occur more frequently than that in the one-dimensional path along *c*-axis.

In an attempt to clarify the origin of the difference in the migration energy barrier among the solute elements, their migration energies were compared with their elemental features, particularly atomic radius and electronegativity. Fig. 4(a,b) shows the dependence of the migration energies of the path with the lowest energy barrier on atomic radius[40] and Pauling's electronegativities [42], which show non-monotonic changes as seen in Fig. 1. For the solute elements N, O and F, the migration energies increased with the increase of the atomic radius. However, for C and B, the migration energy decreased with the increase of the atomic radius. The volcano-like dependence on the electronegativity cannot be simply explained by the bonding ionicity of the solute elements. The diffusion of these interstitial solute elements in α-Ti cannot be simply determined by these simple elemental features.

The electronic structures of the stable and transition states were carefully examined in order to obtain further insight. Fig. 5 shows the projected density of states (PDOS) of the models with the solute atoms at the stable and transition sites. At the stable states, the B- and C-2*p* orbitals mainly interacted with the Ti-3*d* orbitals, whereas the orbitals of the other solute elements were separated in energy and thus localized. This suggests that N, O and F have a more pronounced ionic bonding than that of B and C. Comparing the stable and transition states, the orbitals of C, N, O and F exhibited slight changes, while the B orbital were almost constant. The C-2*p* orbital became slightly delocalized, while the orbitals of O and N shifted toward higher energy side at the transition states. The migration energies of these solute elements are higher than those of B and F, owing to their greater interaction with the host

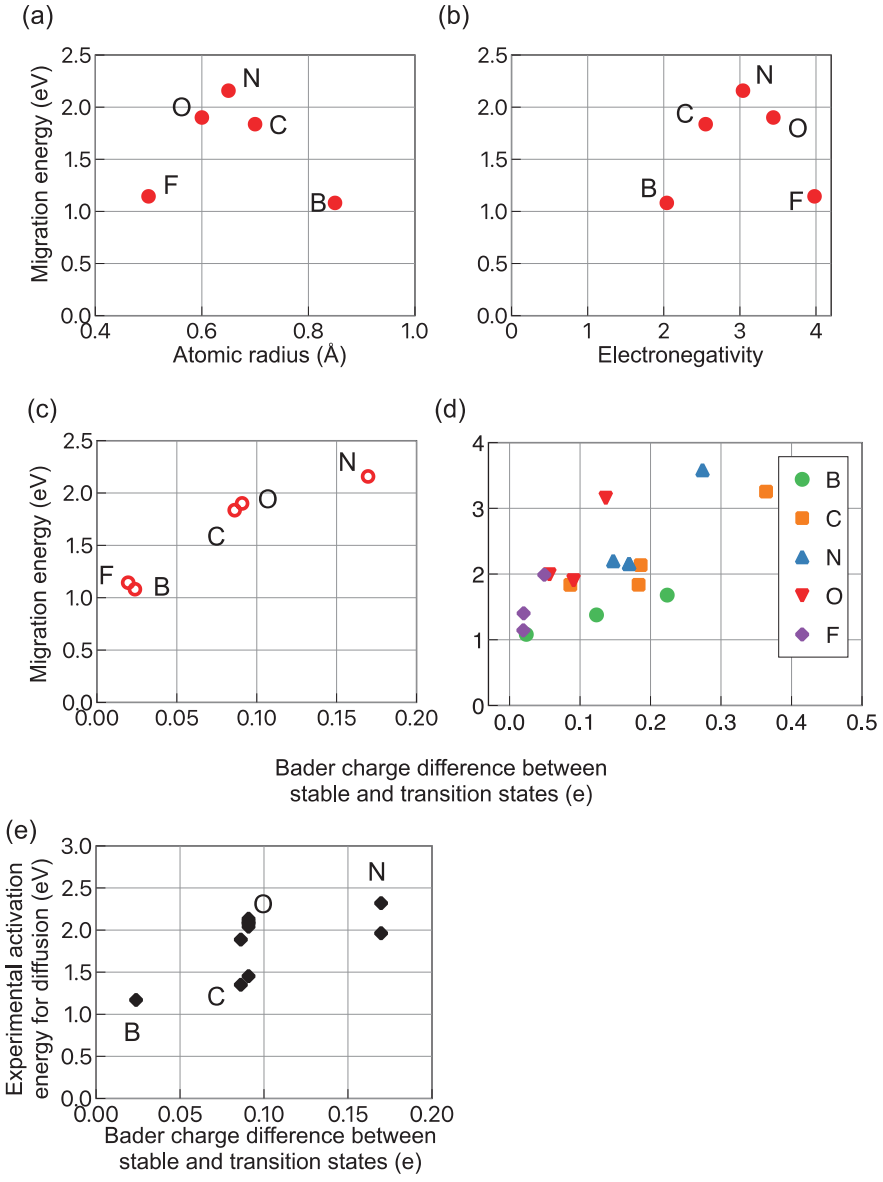

Fig. 4. (a, b) Dependence of the calculated migration energies of the paths with the lowest energy barriers on the (a) atomic radius and (b) Pauling's electronegativity of the solute elements. (c, d) Migration energies for (c) the diffusion paths with the lowest energy barriers and (d) all the paths in terms of the Bader charge difference between the stable and transition states. (e) Experimental activation energies for diffusion [25,26,30–36,38,41] as a function of the Bader charge difference between the stable and transition states of the diffusion paths with lowest migration energy.

Ti atoms at their respective transition states. We also compared the charge density of solute N and F (Figure S2), which exhibit the high and low migration energies, respectively. At the stable states, these solute atoms exhibit an ionic bonding, corresponding to the PDOS results in Fig. 5. However, at the transition states, there are different modifications in the electronic structures between these solute atoms. The interatomic Ti–F bond remained ionic even at the transition state. On the other hand, the interatomic Ti–N bond became more covalent at the transition states.

The Bader charge analysis [59,60] was performed for the stable and transition states to more quantitatively investigate the relationship between the migration energy barrier and local electronic structures. Fig. 4(c) shows the migration energy dependence on the Bader charge difference between the stable and transition states along the paths with the lowest energy barriers for each solute element, which are dominant in diffusion. The difference in charge transfers between the stable and transition states almost linearly affected the migration energy during the diffusion of the interstitial solute elements. Fig. 4(d) shows the migration energy dependence on the charge difference for all the paths considered in this study. Even considering all the diffusion paths, a nearly linear relationship was obtained, implying the anisotropy of the diffusion of these elements were also related with the charge transfer. This quantitative analysis is consistent with the physical insight discussed above. The migration energies of the solute atoms could not be elucidated by the ionic bonds or atomic radius at the stable states alone, instead it can be attributed to the charge transfer between the transition and stable states. For the comparison with experimental values, Fig. 4(e) shows the experimental activation energy [25,26,30–36,38,41] as a function of the Bader charge difference between the stable and transition states of the diffusion path with lowest migration energy. This charge transfer shows almost linear relationship with the experimental values.

The solute diffusion mechanism in α-Ti was quantitively investigated for interstitial solute elements using the first-principles calculations. It was confirmed that the solute atoms B, C, N, O and F

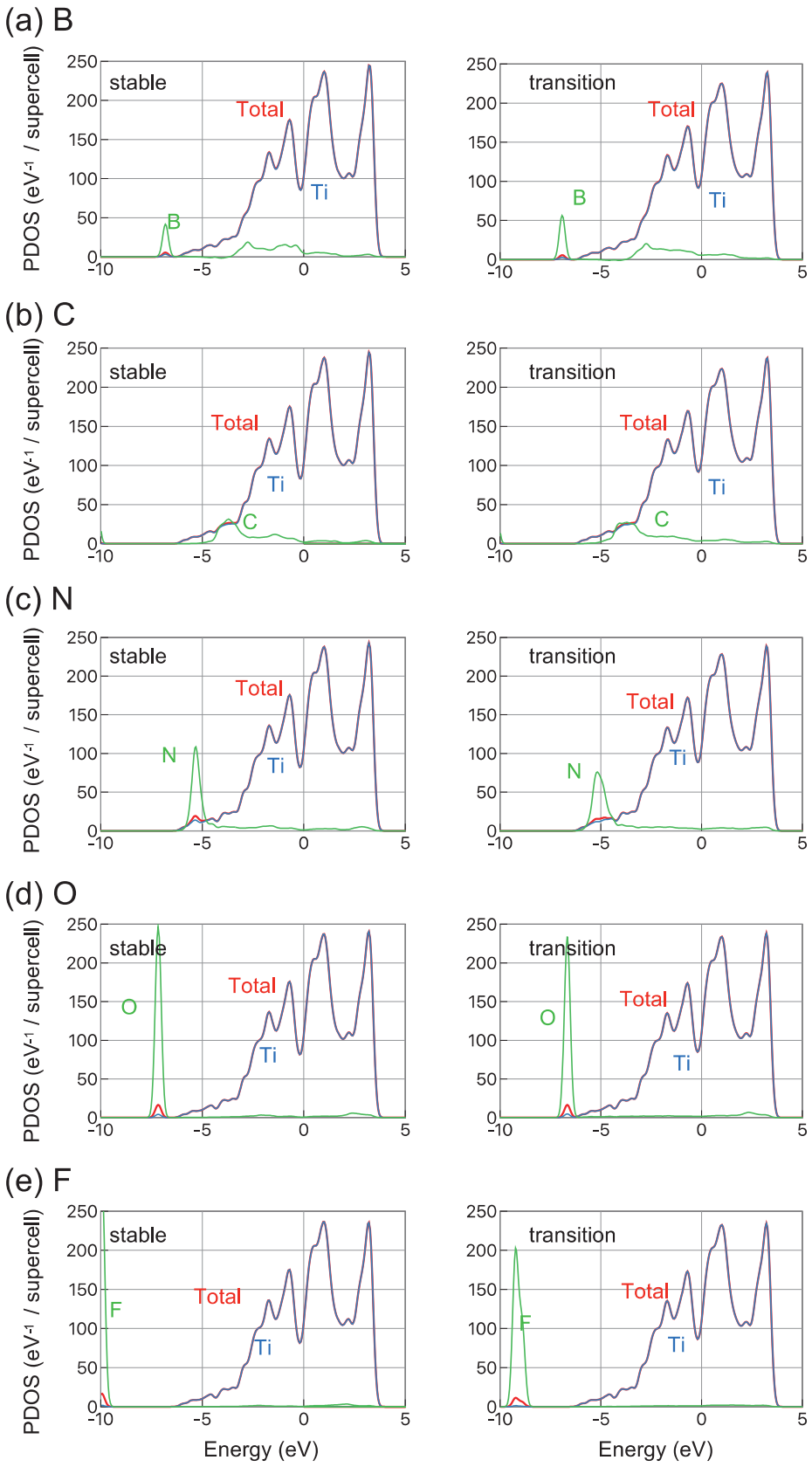

Fig. 5. Total and projected density of states (PDOS) in the stable (left) and transition (right) states for (a) pure Ti, and Ti with (b) B, (c) C, (d) N, (e) O and (f) F atoms. The PDOSs of the solute atoms were multiplied by twenty. At the stable states, the orbitals of B and C interacted with the Ti orbital, thereby forming a covalent bond, while those of the other solutes were separated by the Ti orbitals, thereby resulting in a more ionic bond. Between the stable and transition states, the orbitals of C, N and O displayed slight changes, while B and F orbitals showed almost no changes.

were the most stable at the octahedral sites. The solutes elements C, N and O had high migration energies of approximately 2 eV in α-Ti, while those of B and F were approximately 1 eV, which are consistent with the experimental reports of the activation energies of diffusion for B, C, N and O. The migration energies were dominated by the difference in the charge densities of the solute atoms at the stable and transition states for not only the paths with the lowest energies for each solute element, but also all the diffusion paths. This implies that the anisotropy of solute diffusion is also related the charge transfer between the solute and Ti. These results indicate that the atomic radius or electronegativity of the solute atoms alone cannot explain their migration energies during diffusion. Instead, the charge transfer between the solute and Ti atoms in the course of diffusion should also be considered. In addition, this implies that diffusion can be altered at the grain boundaries where atomic arrangement is modified, or in the vicinity of the substitutional metallic elements other than Ti as charge transfer is different.

Declaration of Competing Interest

The authors declare that they have no known competing financial interests or personal relationships that could have appeared to influence the work reported in this paper.

Acknowledgements

This work was partially supported by the Council for Science, Technology and Innovation, Cross-ministerial Strategic Innovation Promotion Program (SIP), “Materials Integration for revolutionary design system of structural materials” (Funding agency: JST). MY was in part supported by Grant-in-Aid for Scientific Research on Innovative Areas ‘New Materials Science on Nanoscale Structures and Functions of Crystal Defect Cores’ from the Japan Society for the Promotion of Science (JSPS) [grant number 19H05786]. Crystal structures were drawn using the VESTA code [61].

Supplementary materials

Supplementary material associated with this article can be found, in the online version, at doi:10.1016/j.scriptamat.2021.114065.

References

[1] H. Conrad, Prog. Mater. Sci. 26 (1981) 123–403.
[2] R.G. Hennig, D.R. Trinkle, J. Bouchet, S.G. Srinivasan, R.C. Albers, J.W. Wilkins, Nat. Mater. 4 (2005) 129–133.
[3] J.C. Williams, E.A. Starke, Acta Mater. 51 (2003) 5775–5799.
[4] T. Seshacharyulu, S.C. Medeiros, W.G. Frazier, Y.V.R.K. Prasad, Mater. Sci. Eng. A 284 (2000) 184–194.
[5] R. Ding, Z.X. Guo, A. Wilson, Mater. Sci. Eng. A 327 (2002) 233–245.
[6] W.S. Lee, C.F. Lin, Mater. Sci. Eng. A 241 (1998) 48–59.
[7] S.L. Semiatin, T.R. Bieler, Acta Mater. 49 (2001) 3565–3573.
[8] L. Thijs, F. Verhaeghe, T. Craeghs, J. Van Humbeeck, J.P. Kruth, Acta Mater. 58 (2010) 3303–3312.
[9] R.I. Jaffee, H.R. Ogden, D.J. Maykuth, Trans. Am. Inst. Minig Metall. Eng. 2 (1950) 1261–1266.
[10] W.L. Finlay, J.A. Snyder, Trans. Am. Inst. Minig Metall. Eng. 2 (1950) 277–286.
[11] S. Kariya, M. Fukuo, J. Umeda, K. Kondoh, Mater. Trans. 60 (2019) 263–268.
[12] T. Saito, T. Furuta, J.H. Hwang, S. Kuramoto, K. Nishino, N. Suzuki, R. Chen, A. Yamada, K. Ito, Y. Seno, T. Nonaka, H. Ikehata, N. Nagasako, C. Iwamoto, Y. Ikuhara, T. Sakuma, Science 300 (2003) 464–467 (80-.).
[13] A. Issariyapat, P. Visuttipitukul, J. Umeda, K. Kondoh, Addit. Manuf. 36 (2020) 101537.
[14] J. Umeda, H. Ishizaka, S. Li, A. Alhazaa, K. Kondoh, J. Alloys Compd. 846 (2020) 156455.
[15] K. Kondoh, E. Ichikawa, A. Issariyapat, K. Shitara, J. Umeda, B. Chen, S. Li, Mater. Sci. Eng. A 795 (2020) 139983.
[16] K. Kondoh, A. Issariyapat, J. Umeda, P. Visuttipitukul, Mater. Sci. Eng. A 790 (2020) 139641.
[17] L. Liang, O.B.M. Hardouin Duparc, Acta Mater. 110 (2016) 258–267.
[18] K. Chou, E.A. Marquis, Acta Mater. 181 (2019) 367–376.
[19] T. Li, D. Kent, G. Sha, L.T. Stephenson, A.V. Ceguerra, S.P. Ringer, M.S. Dargusch, J.M. Cairney, Acta Mater. 106 (2016) 353–366.
[20] W. Xu, E.W. Lui, A. Pateras, M. Qian, M. Brandt, Acta Mater. 125 (2017) 390–400.
[21] E. Brandl, A. Schoberth, C. Leyens, Mater. Sci. Eng. A 532 (2012) 295–307.
[22] A. Ho, H. Zhao, J.W. Fellowes, F. Martina, A.E. Davis, P.B. Prangnell, Acta Mater. 166 (2019) 306–323.
[23] T. Ishimoto, K. Hagihara, K. Hisamoto, S.H. Sun, T. Nakano, Scr. Mater. 132 (2017) 34–38.
[24] R.A. Perez, H. Nakajima, F. Dyment, Mater. Trans. 44 (2003) 2–13.
[25] H. Nakajima, M. Koiwa, ISIJ Int 31 (1991) 757–766.
[26] A. Anttila, J. Räisänen, J. Keinonen, Appl. Phys. Lett. 42 (1983) 498–500.
[27] H.H. Wu, D.R. Trinkle, Phys. Rev. Lett. 107 (2011) 045504.
[28] H.H. Wu, P. Wisesa, D.R. Trinkle, Phys. Rev. B 94 (2016) 014307.
[29] L. Scotti, A. Mottura, J. Chem. Phys. 144 (2016) 0–9.
[30] R.J. Wasilewski, G.L. Kehl, Jounal Inst. Met. 83 (1954) 94.
[31] W.P. Roe, H.R. Palmer, W.R. Opie, Trans. Am. Soc. Met. 52 (1960) 191.
[32] C.J. Rosa, Metall. Trans. 1 (1970) 2517–2522.
[33] M. Dechamps, P. Lehr, J. Less-Common Met. 56 (1977) 193–207.
[34] D. David, E.A. Garcia, X. Lucas, G. Beranger, J. Less-Common Met. 65 (1979) 51–69.
[35] D. David, G. Beranger, E.A. Garcia, J. Electrochem. Soc. 130 (1983) 1423.
[36] V.B. Vykhodets, S.M. Klotsman, T.E. Kurennykh, A.D. Levin, Defect Diffus. Forum 66–69 (1989) 341.
[37] V.B. Vykhodets, T.E. Kurennykh, A.Y. Fishman, Defect Diffus. Forum 143–147 (1997) 79.
[38] F.C. Wagner, E.J. Bucur, M.A. Steinberg, Trans. Am. Soc. Met. 48 (1956) 742.
[39] L. Scotti, N. Warnken, A. Mottura, Acta Mater 177 (2019) 68–81.
[40] J.C. Slater, J. Chem. Phys. 41 (1964) 3199–3204.
[41] S.V. Divinski, F. Hisker, T. Wilger, M. Friesel, C. Herzig, Intermetallics 16 (2008) 148–155.
[42] L.C. Allen, J. Am. Chem. Soc. 111 (1989) 9003–9014.
[43] G. Kresse, J. Furthmüller, Phys. Rev. B - Condens. Matter Mater. Phys. 54 (1996) 11169–11186.
[44] G. Kresse, D. Joubert, Phys. Rev. B 59 (1999) 1758–1775.
[45] G. Kresse, J. Hafner, Phys. Rev. B 47 (1993) 558–561.
[46] G. Kresse, J. Furthmüller, Comput. Mater. Sci. 6 (1996) 15–50.
[47] J.P. Perdew, A. Ruzsinszky, G.I. Csonka, O.A. Vydrov, G.E. Scuseria, L.A. Constantin, X. Zhou, K. Burke, Phys. Rev. Lett. 100 (2008) 136406.
[48] H.J. Monkhorst, J.D. Pack, Phys. Rev. B 13 (1976) 5188–5192.
[49] A.I. Gusev, A.A. Rempel, Dokl. Akad. Nauk 332 (1993) 717–721.
[50] G. Henkelman, H. Jónsson, J. Chem. Phys. 113 (2000) 9978–9985.
[51] G. Henkelman, B.P. Uberuaga, H. Jónsson, J. Chem. Phys. 113 (2000) 9901–9904.
[52] H.H. Wu, D.R. Trinkle, J. Appl. Phys. 113 (2013) 223504.
[53] K. Shitara, T. Moriasa, A. Sumitani, A. Seko, H. Hayashi, Y. Koyama, R. Huang, D. Han, H. Moriwake, I. Tanaka, Chem. Mater. 29 (2017) 3763–3768.
[54] H. Ubukata, T. Broux, F. Takeiri, K. Shitara, H. Yamashita, A. Kuwabara, G. Kobayashi, H. Kageyama, Chem. Mater. 31 (2019) 7360–7366.
[55] A. O'Hara, A.A. Demkov, Appl. Phys. Lett. 104 (2014) 211909.
[56] A. Kushima, B. Yildiz, J. Mater. Chem. 20 (2010) 4809.
[57] L.J. Zhang, Z.Y. Chen, Q.M. Hu, R. Yang, J. Alloys Compd. 740 (2018) 156–166.
[58] K. Shitara, A. Kuwabara, K. Hibino, K. Fujii, M. Yashima, J.R. Hester, M. Umeda, N. Nunotani, N. Imanaka, Dalt. Trans. 50 (2021) 151–156.
[59] G. Henkelman, A. Arnaldsson, H. Jonsson, Comput. Mater. Sci. 36 (2006) 354–360.
[60] M. Yu, D.R. Trinkle, J. Chem. Phys. 134 (2011) 1–8.
[61] K. Momma, F. Izumi, J. Appl. Crystallogr. 41 (2008) 653–658.